Jordan Journal of Civil Engineering, Volume **20**, No. **3**, **2026**
DOI: https://doi.org/10.14525/JJCE.v20i3.10

Jordan Journal of Civil Engineering

Journal homepage: https://jjce.just.edu.jo

Point Cloud Registration of Ancient Buildings Based on Multi-Source Hybrid Filtering and PCA-ICP

Hua Deng [1)]

[1)] *Department of Management, Chengyi College, Jimei University, Xiamen, 361021, China. Email: denghua0927@126.com*

ARTICLE INFO

Article History:
Received: 4/9/2025
Accepted: 31/3/2026

ABSTRACT

This study addresses noise and registration inaccuracies in multi-source point cloud data to improve digital preservation of ancient buildings. An integrated framework is proposed combining hybrid filtering (octree voxel grids, cloth simulation, and statistical filtering) with improved Principal Component Analysis - Iterative Closest Point (PCA-ICP) registration. The enhanced PCA establishes coarse alignment through principal axis correction, followed by ICP refinement. Hybrid filtering reduced point cloud volume to 15.15% (unstructured) and 91.36% (ordered). On ModelNet40, the proposed method achieved 98.12% precision and 97.55% recall, surpassing traditional PCA by 6.31%. For large-scale data, it achieved 0.1954m root mean square error in 882.56s. The method effectively enhanced point cloud processing efficiency and registration accuracy, offering a viable solution for ancient building digitization.

Keywords: Hybrid filtering, Improved principal component analysis, Computer vision, Point cloud registration, Ancient buildings.

INTRODUCTION

As physical carriers of historical culture, ancient buildings require digital preservation for heritage transmission and structural restoration. The widespread use of 3D laser scanning and UAV oblique photography provides massive point cloud data for high-precision 3D reconstruction of ancient buildings (Shen et al., 2023). However, data from multi-source heterogeneous sensors exhibit varying noise characteristics and resolution differences, leading to registration deviations that compromise reconstruction accuracy and consistency (Wei et al., 2022; Groumpos, 2023). For instance, LiDAR data offers high coordinate accuracy and environmental robustness, but is prone to dense outliers. UAV image-based point clouds are cost-effective with wide coverage, yet their accuracy is sensitive to lighting and texture, often causing data gaps in occluded or low-texture areas (Hu & Sun, 2023). Temporal changes, such as vegetation growth or temporary obstructions, further complicate multi-source data registration.

In point cloud filtering, various methods have been developed for noise removal. Zhang et al. (2024) applied octree downsampling and Cloth Simulation Filtering (CSF) to effectively denoise maglev track point clouds (Zhang et al., 2024). He et al. (2024) divided underwater regions using normal vectors and echo intensity differences, enhancing denoising accuracy with Grubbs test (He et al., 2024). Abdul-Jabbar (2024) proposed Bayesian filtering, integrating prior probability and likelihood function, outperforming single-filter approaches (Abdul-Jabbar, 2024). Sun and Wang (2024).

improved filtering stability via non-parametric clustering and manifold distance truncation to eliminate outliers (Sun & Wang, 2024). However, traditional single-filter methods struggle to balance noise removal with preservation of geometric features in ancient buildings, while CSF under-performs in low-texture areas (Chen et al., 2024). For point cloud registration, research focuses on improving alignment accuracy and efficiency for multi-source data. Liu et al. (2024) accelerated Iterative Closest Point (ICP) registration via dynamic overlap loss and spatial attention encoders (Liu et al., 2024). Huang et al. (2024) enhanced search efficiency and robustness through a three-stage decomposition strategy that re-parameterized high-dimensional problems into lower-dimensional sub-problems (Huang et al., 2024). Li et al. (2024) maintained registration efficiency under high outlier ratios using a screw theory-based decoupling strategy combined with branch-and-bound and global voting (Li et al., 2024). Although the ICP algorithm offers high precision, it is sensitive to initial pose and prone to local optima. Traditional Principal Component Analysis (PCA) methods suffer from eigenvector direction ambiguity, potentially causing incorrect principal axis alignment (Zhao et al., 2024).

In summary, despite significant progress in point cloud filtering and registration, challenges remain in handling multi-source ancient building point clouds, including insufficient adaptability to heterogeneous data, local optima due to initial pose sensitivity, and the difficulty of balancing denoising with feature preservation. Furthermore, the accuracy of ancient building documentation is influenced by multiple practical factors, including building scale, complexity of decorative details, and completeness of source data. Large structures lead to dramatic increases in point cloud volume and density variations, while fine decorations (e.g. dougong, carvings) are prone to erroneous removal during filtering. Data gaps or occlusions further exacerbate registration difficulties. To address these issues, this study proposes an integrated approach combining multi-source hybrid filtering with improved PCA-ICP registration. To address the principal axis ambiguity in traditional PCA caused by limited feature overlap in cross-source point clouds, this study introduces improvements: a contour feature point screening mechanism using CSF and Canny edge detection to extract main building outlines and exclude non-overlapping regions; replacement of the point cloud centroid with the bounding box center of contour points as the PCA origin to enhance spatial reference consistency; and a principal axis sign correction strategy that detects and flips reversed eigenvectors, resolving registration deviations from eigenvector direction uncertainty.

METHODS AND MATERIALS

Point Cloud Data Processing Based on Multi-Source Hybrid Filtering

3D point cloud data is primarily acquired through multi-source heterogeneous sensors, such as multispectral cameras and LiDAR. This data often contains noise points and outliers due to environmental factors and device limitations, increasing computational load and reducing data accuracy (Ismail et al., 2021). To address characteristics of UAV-mounted multispectral camera and ground LiDAR data, distinct filtering processes are applied, as shown in Figure 1.

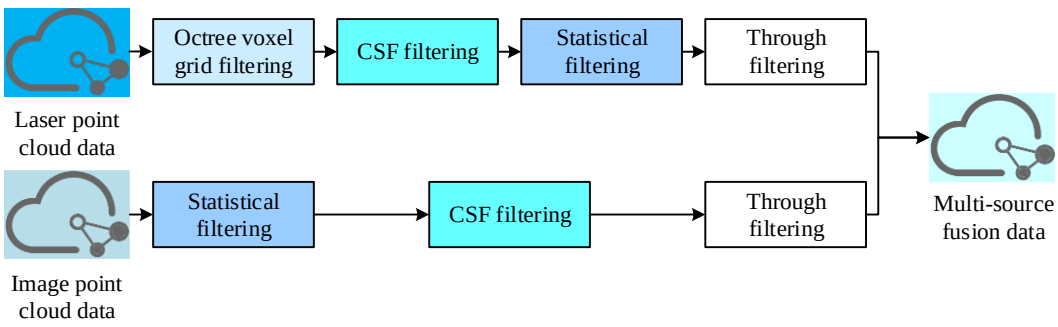

Figure 1. Multi-source hybrid filtering process

As shown in Figure 1, both ordered point clouds from UAV oblique photogrammetry and unstructured point clouds from terrestrial laser scanning undergo hybrid filtering. LiDAR point clouds typically exhibit large volume and discrete spatial distribution due to scanning principles, lacking global spatial indexing. To address this issue, an Octree Voxel Grid (OVG) filter reconstructs the point cloud and establishes a hierarchical topological index model (Wang et al., 2024). Each subdivided voxel unit undergoes downsampling by selecting the point closest to the voxel center. Since the data contains non-architectural elements, like utilities, pedestrians, and vehicles, CSF separates ground point from non-ground points to remove interference while preserving main structures (Huang & Zhao, 2024). CSF demonstrates strong terrain adaptability with simple parameter configuration. For residual local noise in non-ground points after CSF, statistical filtering is applied for further denoising.

Traditional statistical filtering often mistakenly removes fine structures (e.g. dougong, carvings) in ancient building scenarios while being sensitive to noise from weathered surfaces and vegetation. To address this issue, A Curvature-Weighted Adaptive Statistical Filter (CWASF) is proposed, operating through three collaborative stages—feature perception, dynamic processing, and intelligent decision-making—to achieve feature-preserving denoising. The feature perception layer computes point cloud curvature characteristics by decomposing local covariance matrices. Specifically, for any point p_i in the point cloud, a spherical neighborhood $N(i) = \{p_j \mid \| p_j - p_i \| < r_{init}\}$ is reconstructed with it as the center (initial radius $r_{init} = 0.3$m), and the covariance matrices C_i of neighboring points are computed as shown in equation (1).

$$\mathbf{C}_i = \frac{1}{|N(i)|} \sum_{j \in N(i)} (p_j - \bar{p})(p_j - \bar{p})^T \quad (1)$$

In Equation (1), $\bar{p} = \frac{1}{|N(i)|} \sum_{j \in N(i)} p_j$ is the centroid of the neighborhood, $|N(i)|$ is the number of points within the neighborhood *N(i)*, p_j is the j-th point within the neighborhood *N(i)*. The eigenvalue decomposition of C_i is shown in Equation (2).

$$\mathbf{C}_i = \mathbf{V}_i \mathbf{\Lambda}_i \mathbf{V}_i^T, \quad \mathbf{\Lambda}_i = \begin{pmatrix} \lambda_1^{(i)} & 0 & 0 \\ 0 & \lambda_2^{(i)} & 0 \\ 0 & 0 & \lambda_3^{(i)} \end{pmatrix} \quad (2)$$

In Equation (2), $\mathbf{\Lambda}_i$ is a diagonal matrix, $\mathbf{V}_i^T$ is a 3×3 orthogonal matrix, and $\lambda_1^{(i)}, \lambda_2^{(i)}, \lambda_3^{(i)}$, are eigenvalues satisfying $\lambda_1^{(i)} \geq \lambda_2^{(i)} \geq \lambda_3^{(i)}$. These eigenvalues describe the dispersion degree of the point cloud along the principal direction. The curvature κ_i is then calculated based on these eigenvalues, as shown in Equation (3).

$$\kappa_i = \lambda_3^{(i)} / (\lambda_1^{(i)} + \lambda_2^{(i)} + \lambda_3^{(i)}) \quad (3)$$

Equation (3) employs normalized curvature features to characterize the normal variation rate of point cloud surfaces. When $\kappa_i \approx 0$ is low, indicating relatively flat terrain, the region can be processed for noise reduction. Conversely, when $\kappa_i > 0.1$ is high, the area may contain structural elements, like dougong brackets or flying eaves in ancient architecture, requiring robust filtering to preserve features. In the dynamic processing layer, we dynamically adjust the neighborhood radius based on curvature κ_i , as demonstrated in Equation (4).

$$r(\kappa_i) = r_{\min} + \frac{r_{\max} - r_{\min}}{1 + e^{-\beta(\kappa_i - \kappa_0)}} \quad (4)$$

In Equation (4), $r(\kappa_i)$ denotes the dynamic neighborhood radius of point p_i, where $r_{\min} = 0.05$ and $r_{\max} = 0.3$ represent the minimum and maximum neighborhood radii, respectively, which are mapped through a Sigmoid function based on curvature characteristics. Here, $\beta = 30$ denotes the Sigmoid slope coefficient, while $\kappa_0 = 0.05$ serves as the curvature threshold that triggers radius adjustments. After determining the neighborhood radius, the weighted distance $\tilde{d}_j$ is calculated for each point p_j within the neighborhood to reduce the risk of feature point misidentification, as shown in Equation (5).

$$\tilde{d}_j = \| p_i - p_j \| \cdot w(\kappa_j), w(\kappa_j) = 1 + \alpha \cdot \tanh(\gamma \kappa_j) \quad (5)$$

In Equation (5), $w(\kappa_i)$is the curvature weighting function, and α and γ are amplitude coefficient and curvature sensitivity coefficient, respectively, which are 1.8 and 12. The dynamic determination of outliers in the intelligent decision layer is shown in Equation (6).

$$\min_j \tilde{d}_j > \mu_{\text{adapt}} + \tau(\kappa_i)\cdot\sigma_{\text{adapt}}, \tau(\kappa_i) = \tau_{\min} + (\tau_{\max} - \tau_{\min})\cdot\frac{1-\cos(2\pi k\kappa_i)}{2} \quad (6)$$

In Equation (6), μ_{adapt} and σ_{adapt} represent the mean and standard deviation of weighted distances, respectively. The threshold function $\tau(\kappa_i)$ converts curvature features into statistical criteria scaling factors to align with the periodic characteristics of ancient architectural structures. c and $\tau_{\max}$ are the minimum and maximum threshold multiples, respectively, which are 1.2 and 1.8. k = 4 serves as the periodicity control parameter. For ordered point clouds from image matching, which have smaller data volume with sparse, near-ground noise distribution, the process skips OVG filtering. It directly applies statistical filtering to remove discrete outliers, uses CSF to refine ground/non-ground separation, and finally applies pass-through filtering for spatial refinement (Janssen et al., 2024; Liu et al., 2023).

Point Cloud Registration Method Based on PCA-ICP

Filtered point clouds still inadequately represent architectural spatial states, requiring registration to integrate camera and LiDAR data into a unified coordinate system. The ICP algorithm provides high-precision registration via least squares, iteratively finding correspondences and updating transformation matrices until convergence. However, ICP is sensitive to initial pose and may converge to local minima with large initial misalignments. To address this issue, we employ improved PCA for coarse registration to obtain better initial poses. Limited overlap in cross-source point clouds causes traditional PCA to miscalculate centroids and principal axes due to distribution differences in non-overlapping areas. The study mitigates this problem by: 1) extracting contour feature points via CSF filtering and Canny edge detection, retaining only structural points for PCA to avoid non-overlapping region interference; 2) using the minimum bounding box center of contour points as the PCA origin instead of the point cloud centroid, ensuring consistent spatial reference between source and target point clouds. The coarse registration workflow is shown in Figure 2.

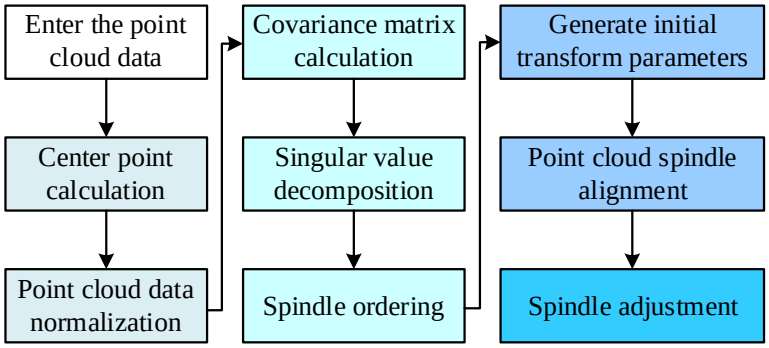

Figure 2. The coarse registration workflow

As shown in Figure 2, after inputting point cloud data, it is necessary to determine the centroids $\bar{E}$ and $\bar{F}$ of the source point cloud E and the target point cloud F. The calculation of the center of mass is shown in Equation (7).

$$\bar{E} = \frac{1}{q}\sum_{i=1}^{q} e_i, \bar{F} = \frac{1}{u}\sum_{i=1}^{u} f_i \quad (7)$$

In Equation (7), q and u, respectively, represent the total number of source point cloud and target point clouds. e_i and f_i are the data points in the point cloud. Afterwards, the point cloud data is normalized to fall into the PCA coordinate system (Wang & Bao, 2021). Subsequently, the covariance matrix of $\bar{E}$ and $\bar{F}$ is computed, and singular value decomposition is performed. After the above operation, the vector in the principal axis direction in the PCA coordinate system is obtained. To align the principal axis of the point cloud and place it in the same coordinate system, it is necessary to calculate the initial rigid body transformation parameters according to Equation (8) (Morita, 2024).

$$B = \bar{F} - R\bar{E}, R = M_e W_f^T \quad (8)$$

In Equation (8), B is the translation vector (describing the linear offset between the source and target point clouds), R is the rotation matrix (a 3×3 orthogonal matrix that aligns the principal directions of the two point clouds), and M_e and W_f^T are orthogonal matrices obtained from the singular value decomposition of the covariance matrices of the source and target point clouds, respectively. The point cloud registration types obtained through the above operation are shown in Table 1.

Table 1. Correspondence of the principal axis direction of the point cloud

	Sequence number	Target point cloud main coordinate axis		
		$W_f(x)$	$W_f(y)$	$W_f(z)$
Source point cloud coordinate axis	1	$W_e(x)$	$W_e(x)$	$W_e(x)$
	2	$-W_e(x)$	$W_e(x)$	$W_e(x)$
	3	$W_e(x)$	$-W_e(x)$	$W_e(x)$
	4	$W_e(x)$	$W_e(x)$	$-W_e(x)$
	5	$-W_e(x)$	$-W_e(x)$	$W_e(x)$
	6	$-W_e(x)$	$W_e(x)$	$-W_e(x)$
	7	$W_e(x)$	$-W_e(x)$	$-W_e(x)$
	8	$-W_e(x)$	$-W_e(x)$	$-W_e(x)$

Table 1 presents eight-point cloud registration types, enhancing coarse registration robustness through diversity to address opposing coordinate axes between source and target point clouds. In summary, the processing flow for multi-source point cloud hybrid filtering and improved PCA-ICP registration is shown in Figure 3.

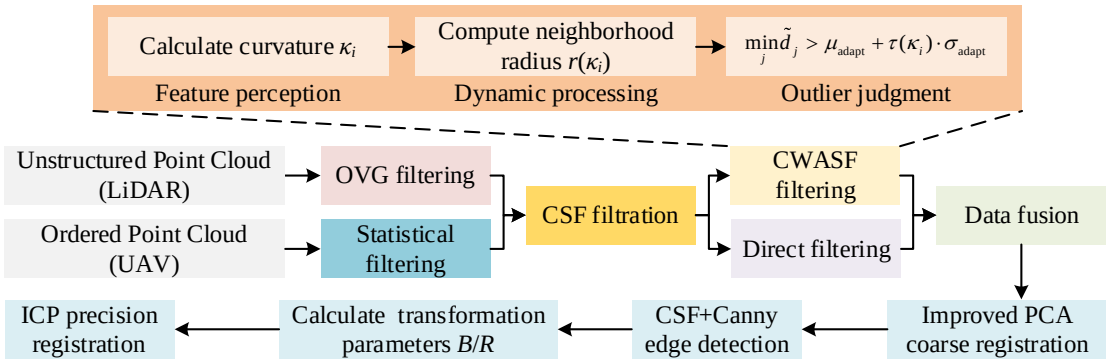

Figure 3. Processing flow for multi-source point cloud hybrid filtering and improved PCA-ICP registration

Figure 3 presents the complete processing pipeline for multi-source point clouds, from preprocessing to accurate registration, with differentiated filtering pathways designed according to the characteristics of unstructured (LiDAR) and ordered (UAV) point clouds. Specifically, unstructured point clouds are first processed by OVG filtering, which simplifies the data through voxel-grid downsampling; then, CSF filtering is applied to separate ground points and non-ground points, removing environmental interference; finally, CWASF filtering is employed to simultaneously suppress noise and preserve fine architectural features (e.g. dougong brackets and carvings). In contrast, ordered point clouds undergo statistical outlier removal first to eliminate discrete noise, followed by CSF filtering with identical parameters to optimize terrain-

object separation, and finally pass-through filtering to refine the spatial extent. After both point cloud types are transformed into a unified coordinate system, an improved PCA-based method performs coarse registration, followed by point-to-plane ICP for fine registration to minimize local alignment errors, ultimately yielding the filtered and accurately aligned point cloud output.

RESULTS

Analysis of the Data Reduction Rate of Multi-Source Hybrid Filtering Method

To determine optimal filtering parameters, we compared method performance under different settings. Ground LiDAR data was acquired via laser ranging, while UAV data was generated using Structure from Motion and Multi-View Stereo algorithms in Context Capture. Image overlap was maintained ≥80% with optimized camera calibration to ensure point cloud quality. The original dataset contained 7.1725×10^8 points from laser scanning and 7.8336×10^7 points from UAV photogrammetry. Experiments used an Intel i5-7300HQ desktop with MATLAB R2024. Filtering results for unstructured point clouds are shown in Table 2.

Table 2. Results of filtering by different methods

Filtering method	Parameter setting	Number of point clouds	Filter effect
OVG filtering	G=20	7.1683×10^8	0.0575%
	G=14	1.3168×10^8	81.64%
	G=10	9.3959×10^6	98.69%
	G=9	1.4345×10^5	99.98%
CSF	H=0.5	1.2458×10^7	12.45%
	H=0.25	9.7435×10^7	9.74%
	H=0.1	7.3672×10^7	7.36%
	H=0.05	7.1379×10^7	7.13%
Through filtering	$\triangle h$=40cm	7.1762×10^7	0.19%

From Table 2: When the maximum segmentation layer G of OVG was 9 or 10, filtering efficiency exceeded 98%, but the point cloud could not fully describe the building shape. Setting G to 11-13 yielded a small point cloud with blurry building details. Thus, G=14 was selected, as its point cloud well preserved building details. In CSF: When height threshold H was 0.5-0.1, residual artifacts existed; H=0.05 caused many ground defects. Comparing H=0.09 and 0.08: H=0.09 performed better, while H=0.08 left ground gaps. Hence, H=0.09 was chosen. To verify CWASF's effectiveness, 5 ancient building point cloud samples (density: 200-500 points/m², with 0.02-0.05mm Gaussian noise and system errors) were used. Traditional statistical filtering (neighborhood radius: 0.15m, standard deviation multiple: 3.0) was compared with improved CWASF. Each sample ran 10 times independently (results averaged) to evaluate noise removal rate and feature point retention rate. Their performance comparison (before/after improvement) is shown in Table 3.

Table 3. Comparison of noise removal rate and feature point retention rate of point clouds from different samples

Sample No.	Traditional statistical filtering		Improved CWASF	
	Noise removal rate (%)	Feature point retention rate (%)	Noise removal rate (%)	Feature point retention rate (%)
1	92.45	67.32	91.78	89.56
2	93.12	69.45	92.56	90.12
3	91.87	71.23	91.03	88.78
4	90.56	65.78	89.89	91.34
5	92.78	68.91	92.15	89.87

From Table 3: In terms of noise removal, the noise removal rate of traditional statistical filtering was

slightly higher overall than that of the improved method—mean values for Samples 1–5 were 92.16% and 91.48%, respectively, with an average difference of ~0.68%. However, in feature point preservation, CWASF performed significantly better: its mean feature point retention rate reached 89.93%, ~21.39% higher than the traditional method's 68.54%. Overall, by sacrificing 0.6%-0.8% of noise removal rate, CWASF gained over 20% improvement in feature point retention rate, making it more suitable for processing ancient building point clouds (scenarios involving both noise interference and complex features). Using CWASF to process the initial ancient building data, the filtering efficiency here was 5.843%. In pass-through filtering, setting $\triangle h$ to 40 removed point clouds in the selected area, with a data reduction rate of 0.1923%. Finally, combining the filtered ground point and non-ground point cloud data gave a point cloud count of 1.0732×10^8, a data reduction rate of 84.6426%, and a 72.4632% reduction in storage space occupancy. Similarly, filtering the ordered point cloud yielded a count of 7.0531×10^7, a data reduction rate of 86.1146%, and a 5.7462% reduction in storage space occupancy.

Performance Analysis of Point Cloud Registration Algorithm

To validate the improved PCA, the study compared its registration performance against Sample Consensus Initial Alignment (SAC-IA) and 4-Point Congruent Sets (4PCS). On the ModelNet40 dataset, the improved PCA achieved 98.34% precision (6.09% higher than traditional PCA) and 97.55% recall (surpassing 4PCS, SAC-IA, and PCA by 5.42%, 4.99%, and 6.17%) after 250 iterations. It stabilized after only 75 iterations, while other methods required over 150 iterations, demonstrating superior efficiency without compromising accuracy. The changes in root mean square error (RMSE) of different coarse registration methods and ICP fine registration methods in point cloud data of different numbers of ancient buildings are shown in Figure 4.

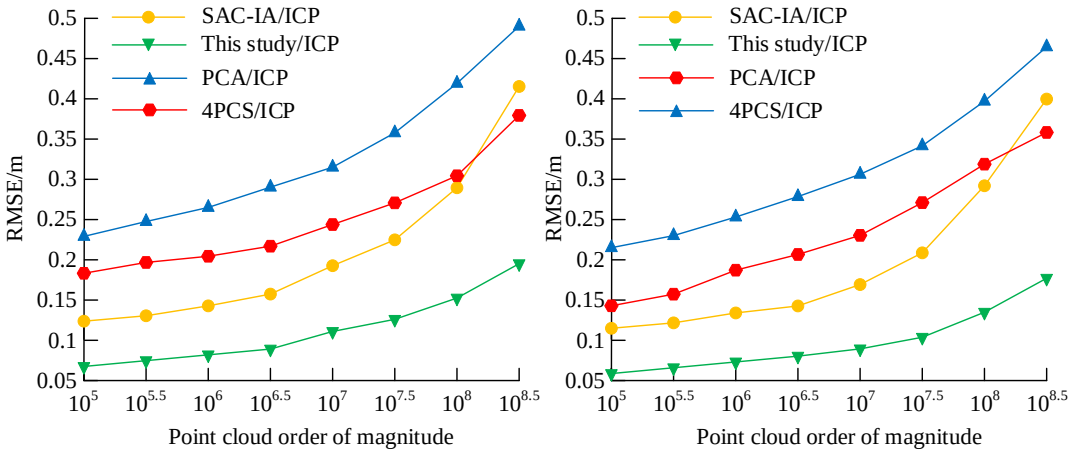

(a) RMSE changes of each coarse registration method combined with ICP (point-to-point)

(b) RMSE changes of each coarse registration method combined with ICP (point-to-surface)

Figure 4. RMSE of different coarse registration methods and ICP fine registration methods in different numbers of point cloud data

As shown in Figure 4 (a), the improved PCA with point-to-point ICP achieved the lowest RMSE across varying point cloud scales, reaching 0.1954m at $10^{8.5}$ points - representing reductions of 0.2282m, 0.1774m, and 0.2812m compared to SAC-IA, PCA, and 4PCS, respectively. While 4PCS enhanced robustness through global sampling, it remained sensitive to point density variations. The 4PCS/ICP combination tended to produce registration deviations with uneven density due to its reliance on global sample consistency. Figure 4 (b) demonstrates that combining coarse registration with point-to-plane ICP further reduced RMSE, making it preferable for alignment accuracy. Comparison of point cloud registration runtime showed that the improved PCA + point-to-point ICP was more efficient. At $10^{8.5}$ data volume, its runtime was only 882.56s—

749.79s/820.09s shorter than SAC-IA/PCA, respectively. This was because it quickly identified key points via local geometric properties, without complex global optimization.

In contrast, point-to-plane ICP involved more complex geometric calculations (needing to compute point-to-plane distances per iteration), so its runtime increased when combined with any rough registration method. SAC-IA took the longest, as it needed to identify numerous descriptor pairs. To evaluate the method's effectiveness in real-world heritage digitization and explore limitations from structural complexity, scale, and environmental conditions, experiments were conducted on five representative ancient buildings, including Yingxian Wooden Pagoda (timber structure) and Fujian Tulou (rammed earth building), covering complex timber, masonry, and earthen architectures. The processing results for each structure are shown in Table 4.

Table 4. Filtering and registration results of point clouds from different ancient buildings

Case Name	**Original Point Count (107)**	**Filtered Point Count (107)**	**Data reduction rat (%)**	**Registration RMSE (m)**	**Registration Time (s)**
Yingxian Wooden Pagoda	68.40	10.70	84.36	0.2145	927.89
Fujian Tulou	0.832	0.765	88.05	0.1887	757.64
Pingyao Ancient City Wall	64.70	1.18	81.76	0.1558	1026.38
Yuanxiang Hall of Humble Administrator's Garden	0.478	0.119	75.1	0.2025	725.93
Mogao Grottoes Cave 254	52.9	9.40	82.23	0.1776	959.42

The results in Table 4 demonstrate this method's strong performance on geometrically regular structures, like Fujian Tulou (88.05% data reduction rate, 0.1887m RMSE). For complex architectures, such as Yingxian Wooden Pagoda and Yuanxiang Hall, where vegetation occlusion and visitor interference exist, the method maintained a trade-off between filtering efficiency (75.1%-84.36%) and registration accuracy to preserve delicate features. Although the massive point cloud from Pingyao Ancient City Wall increased processing time to 1026.38s, the method maintained controlled efficiency while adapting to various architectural digitization requirements.

CONCLUSIONS

To mitigate noise interference, registration inaccuracies, and storage inefficiencies in ancient architecture point cloud processing, this study integrated multi-source hybrid filtering with improved PCA-ICP registration. The approach achieved 72% storage savings while maintaining 0.012° angular accuracy, demonstrating scalability for ancient building digitization. Experimental results showed data reduction rate of 84.8491% (unstructured) and 86.3332% (ordered), with improved PCA achieving 98.12% precision and 97.55% recall on ModelNet40. The superior feature retention of CWASF stemmed from its curvature-aware mechanism, which dynamically adjusted the neighborhood radius and weighted distance. By adopting a conservative filtering strategy in high-curvature areas (e.g. dougong, carvings), it effectively balanced noise suppression and structural integrity. Compared to the fixed parameters of traditional statistical filtering, CWASF exhibited local adaptability, making it more suitable for the complex geometry of heritage structures. In contrast to learning-based registration methods (e.g. deep feature matching), the proposed approach required no large-scale annotated data, offering greater practicality and interpretability in data-scarce ancient building scenarios with diverse structures. While being slightly less robust under extreme noise, it achieved higher computational efficiency, making it more suitable for engineering applications.

The proposed framework aligned with recent multi-technique fusion studies (Abdul-Jabbar, 2024; Chen et al., 2024), yet advanced them by explicitly resolving the

feature-preservation challenge in complex heritage structures. The method achieved approximately 21% higher feature retention than traditional statistical filters (Liu et al., 2024). While learning-based approaches (Huang et al., 2024) demonstrated strong robustness, the improved PCA-ICP method provided a data-efficient alternative with superior interpretability, effectively bridging a critical gap between classical algorithms and modern data-driven approaches in ancient building digitization. This balance enhanced the practicality of creating high-fidelity digital archives, crucial for conservation and monitoring. However, the method's efficiency could be influenced by extreme structural scales, where computational demands increased, and by adverse environmental conditions, such as dense vegetation or dynamic occlusions, which may compromise data completeness and initial alignment. Future research will develop a GPU-based parallel computing framework to optimize algorithm parallelism and memory access patterns, improving computational efficiency for large-scale heritage digitization projects.

Funding

The research is supported by Special fund for first-class discipline construction of Chengyi College, Jimei University (2023): Inheritance and innovation of historic buildings in Fujian and Taiwan (NO.C11709).

REFERENCES

AbdulJabbar, S., & Haval. (2024). A Bayesian framework for 3D point cloud filtering. *Journal of Spatial Science, 69*(3), 995-1018.

Chen, T., Qian, X., Lou, P., & Peng, L. (2024). A high-precision point cloud registration method based on graph search Point-to-Tangent ICP. *Robot, 46*(5), 600-610.

Groumpos, P.P. (2023). A critical historic overview of artificial intelligence: Issues, challenges, opportunities, and threats. *Artificial Intelligence and Applications, 1*(4), 197-213.

He, Z., Wu, Y., Li, S., Zhang, S., Li, H., & Bian, S. (2024). A partition filtering method for 3D sonar point cloud data considering horizontal deviation. *Geomatics and Information Science of Wuhan University, 49*(9), 1639-1649.

Hu, E., & Sun, L. (2023). VODRAC: Efficient and robust correspondence-based point cloud registration with extreme outlier ratios. *Journal of King Saud University-Computer and Information Sciences, 35*(1), 38-55.

Huang, T., Li, H., Peng, L., Liu, Y., & Liu, Y. (2024). Efficient and robust point cloud registration via heuristics-guided parameter search. *IEEE Transactions on Pattern Analysis and Machine Intelligence, 46*(10), 6966-6984.

Huang, X., & Zhao, J. (2024). A point cloud filtering algorithm for combining region growth and cloth simulation. *Journal of Geomatics, 49*(5), 24-27.

Ismail, S., Raphael, W., & Durand, E. (2021). Monitoring the Beirut Port silos' structural health response a few months after blast loading using 3D laser scan. *Jordan Journal of Civil Engineering, 15*(3).

Janssen, J., Kuhlmann, H., & Holst, C. (2024). Keypoint-based registration of TLS point clouds using a statistical matching approach. *Journal of Applied Geodesy, 18*(2), 267-284.

Li, X., Ma, Z., Liu, Y., Zimmer, W., Cao, H., Zhang, F., & Knoll, A. (2024). Transformation decoupling strategy based on screw theory for deterministic point cloud registration with gravity prior. *IEEE Transactions on Pattern Analysis and Machine Intelligence, 46*(12), 10515-10532.

Liu, J., Lv, X., Gong, X., Liang, Y., & Hyyppä, J. (2024). An unsupervised learning network for large-scale LiDAR point clouds registration. *IEEE Transactions on Vehicular Technology, 73*(11), 16187-16200.

Liu, Z., Wang, L., Huang, J., Guo, X., Cheng, T., Wang, Y., Liu, C., & Liu, C. (2023). An effective denoising method for the point cloud of trees based on the hybrid filtering scheme. *Automatic Control and Computer Sciences, 57*(5), 504-513.

Morita, K. (2024). Detection of ceiling sagging based on deep learning of images and point clouds. *AIJ Journal of Technology and Design, 30*(74), 165-169.

Shen, Z., Luo, N., Wang, W., & Yang, B. (2023). RANSAC algorithm and distributed framework for point cloud processing of ancient buildings. *Journal of Computing and Information Technology, 31*(2), 107-122.

Sun, Y., & Wang, J. (2024). Nonparametric point cloud filter. *IET Image Processing*, *18*(2), 388-402.

Wang, L., & Bao, J. (2021). Initial registration algorithm for PCA point cloud data with additional main direction decision. *Journal of Geomatics*, *46*(6), 59-62.

Wang, Z., Wan, S., & Wei, L. (2024). Optimized octree codec for geometry-based point cloud compression. *Signal, Image and Video Processing*, *18*(1), 761-772.

Wei, S., Liu, C., Tang, N., Zhao, X., Zhang, H., & Zhou, X. (2022). Indoor and outdoor multi-source 3D data fusion method for ancient buildings. *Journal of Measurements in Engineering*, *10*(3), 117-139.

Zhang, Y., Zhang, L., & Ou, D. (2024). Hybrid filtering method for multisource point cloud data of maglev tracks. *Computer Engineering*, *50*(9), 54-62.

Zhao, W., Zhang, D., Li, D., Zhang, Y., & Ling, Q. (2024). Optimized GICP registration algorithm based on principal component analysis for point cloud edge extraction. *Measurement & Control*, *57*(1), 77-89.